AFRL-AFOSR-UK-TR-2019-0035

Investigating the mystery of the African ionospheric irregularity

Melessew Nigussie
BAHIR DAR UNIVERSITY
Bahir Dar University
Bahir Dar, 100
ET

07/08/2019
Final Report

Air Force Research Laboratory
Air Force Office of Scientific Research
European Office of Aerospace Research and Development
Unit 4515 Box 14, APO AE 09421

REPORT DOCUMENTATION PAGE

Form Approved
OMB No. 0704-0188

1. REPORT DATE *(DD-MM-YYYY)*	2. REPORT TYPE	3. DATES COVERED *(From - To)*
08-07-2019	Final	01 Dec 2015 to 30 Nov 2018

4. TITLE AND SUBTITLE
Investigating the mystery of the African ionospheric irregularity

5a. CONTRACT NUMBER

5b. GRANT NUMBER
FA9550-16-1-0070

5c. PROGRAM ELEMENT NUMBER
61102F

6. AUTHOR(S)
Melessew Nigussie, Baylie Y Damtie

5d. PROJECT NUMBER

5e. TASK NUMBER

5f. WORK UNIT NUMBER

7. PERFORMING ORGANIZATION NAME(S) AND ADDRESS(ES)
BAHIR DAR UNIVERSITY
Bahir Dar University
Bahir Dar, 100 ET

8. PERFORMING ORGANIZATION REPORT NUMBER

9. SPONSORING/MONITORING AGENCY NAME(S) AND ADDRESS(ES)
EOARD
Unit 4515
APO AE 09421-4515

10. SPONSOR/MONITOR'S ACRONYM(S)
AFRL/AFOSR IOE

11. SPONSOR/MONITOR'S REPORT NUMBER(S)
AFRL-AFOSR-UK-TR-2019-0035

12. DISTRIBUTION/AVAILABILITY STATEMENT
A DISTRIBUTION UNLIMITED: PB Public Release

13. SUPPLEMENTARY NOTES

14. ABSTRACT
The variability of the Earth's ionosphere is driven by the sun and the magnetosphere from above and the dynamics of the Earth's atmosphere from below. The variability of the low latitude region, especially the one happening after sunset that is usually called equatorial spread F (ESF), is very complicated and unpredictable. This post-sunset equatorial ionospheric irregularity is a big threat for applications that depend on trans-ionospheric propagating radio waves. Observational studies have shown clear seasonal and longitudinal variability of ESF; peak occurrence rate observed in the American-Atlantic-Africa sector as compared to the other regions; however, the physical mechanism for the occurrence of seasonal and longitudinal variations of the irregularity is not well understood. This project is designed to address potential problems like: what physical mechanism is responsible for the seasonal and longitudinal variations of the equatorial ionospheric irregularity? Is it due to the electrodynamics or atmospheric gravity wave seeding differences? In this project supported by EOARD grant, potential scientific problems related to the variability of equatorial ionosphere have been addressed and about sixteen papers and manuscripts are produced. In addition of the five PhD students supported by this grant one has defended his PhD thesis in February 2019.

15. SUBJECT TERMS
EOARD, ionospheric irregularities, scintillation

16. SECURITY CLASSIFICATION OF:			17. LIMITATION OF ABSTRACT	18. NUMBER OF PAGES	19a. NAME OF RESPONSIBLE PERSON
a. REPORT	b. ABSTRACT	c. THIS PAGE			MILLER, KENT
Unclassified	Unclassified	Unclassified	SAR		19b. TELEPHONE NUMBER *(Include area code)* 011-44-1895-616022

Fianl report of Research Activities done in the framework of EOARD (EOARD Grant FA9550-16-1-0070)

- **Project title**:Investigating the mystery of African ionospheric irregularity
- **Principal Investigator**: Dr Melessew Nigussie
- **Co-Investigator**: Dr Baylie Damtie
- **Affiliation**: Washera Geospace and Radar science research Laboratory (WaGRL), Bahir Dar University, Ethiopia
- **Final report period**: December 2015 to June 2019

Contents

1 Introduction

The variability of the Earth's ionosphere is controlled by the conditions of the sun and magnetosphere from above and the conditions of the Earth's atmosphere from below. The low latitude region of the ionosphere exhibits very complicated and unpredictable variability that affects trans-ionospheric propagating radio wave dependent technologies. The post-sunset equatorial ionospheric irregularity is known by the generic name called equatorial spread F (ESF). It is believed to be triggered by the Rayleigh-Taylor Instability (RTI) mechanism (Sultan, 1996). The growth rate of the irregularity that starts in the bottom-side of the F-layer of the equatorial ionosphere is controlled by different factors such as plasma vertical drift velocity, vertical neutral wind speed, collision frequency between the neutral atmosphere and ions, gravitational acceleration of the Earth, vertical gradient of electron density, integrated conductivity of the ionosphere, and recombination rate and it is expressed mathematically by

$$\gamma_{RT} = \frac{\Sigma^F}{\Sigma^E + \Sigma^F} \frac{\partial N}{\partial h} (\frac{E}{B} - \frac{g}{\nu} + U_n) - R. \quad (1)$$

Vertical drift velocity is identified as the main factor for the occurrence of irregularity (Sultan, 1996). It is directly proportional to Pre-reversal Enhancement (PRE) zonal electric field that is due to evening time F layer ionospheric dynamo and inversely propositional to the Earth's magnetic field strength (Rishbeth, 1971). In addition, the solar terminator geomagnetic field alignment model, proposed by Tsunoda (1985), is able to describe the occurrence of irregularities during the equinox seasons; but it fails to describe the occurrence of irregularities during the solstices seasons. The climatological characteristics of the RTI growth rate and occurrence of equatorial ionospheric irregularity have shwon good agreement. As the RTI model is failed to describe the day-to-day variability of the occurrence of irregularity (Tsunda, 2006; Mendillo et al., 1992), atmospheric gravity wave seeding from below has been proposed as one of the candidates for the cause of the day-to-day variability of the occurrence of ionospheric irregularity (McClure et al., 1998; Tsunda et al., 2010; Kelley et al., 1981). But, apart from proposition, the role of atmospheric gravity wave on seeding the equatorial ionosphere has not yet fully understood. For example, as the atmospheric gravity wave has wide spectrum which range of wavelength gravity waves are responsible for the generation of the equatorial ionosphere. What is the correlation between the characteristics of atmospheric gravity waves and oscillation of equatorial ionosphere irregularity? Different observational studies have also been conducted to characterize the seasonal and longitudinal variability of the equatorial ionospheric irregularity (Hei et al., 2005; Su et al., 2006) and they identified high occurrence of ionospheric irregularities in the American-Atlantic-Africa sector. The correlation between the monthly and longitudinal variability of vertical drift velocity and occurrence of irregularity have been investigated and found good agreement (Huang and Hairston, 2015). But, the causes for the longitudinal variability of vertical drift velocity are not yet fully understood as it depends on different factors. For example, to what extent the longitudinal variability of the zonal neutral wind speed that is believed to be the cause for PRE due ionospheric dynamo (Rishbeth 1971; Eccles et al., 2015) affects the longitudinal variability of the vertical drift velocity? Of the factors that affect the

vertical drift velocity which one is the dominant factor? Is it the zonal neutral wind speed or geomagnetic field strength at the magnetic equator? These questions imply that it is still challenging to understand what physical mechanisms are responsible for the monthly and longitudinal variability of the occurrence of the equatorial ionosphere. What causes the longitudinal and seasonal variability of the occurrence of equatorial ionospheric irregularity? Is it due to different electrodynamics or seeding mechanism (e.g. atmospheric gravity wave)?

It is clear that the effect of the ionosphere on radio wave propagation can be minimized when the characteristics of the ionosphere and variability of its drivers such as solar activity are well known and modeled properly. Therefore, in this project characterization and modeling of variability of the equatorial ionosphere and solar conditions have been done by researchers and PhD students at Washera Geospace and Radar Science Research laboratory at Bahir Dar University, Ethiopia. EOADR Grant FA9550-16-1-0070 has created an excellent opportunity to carrying out investigations to address research questions raised above and other similar questions. The research and educational activities done supported by this grant are described below.

2 Summary of research results

2.1 Characterization of the equatorial ionospheric irregularity

Research questions raised in this project supported by EOARD grant are addressed using data from different sources such as Low Earth Orbiting (LEO) satellites, Global Positioning System (GPS), magnetometers, both ground and space based Fabry-Perot Interferometer (FPI), models, and so on. One of the objectives in this project is to investigate the cause for the seasonal and longitudinal variability of occurrence of equatorial spread F. This research question has been addressed using data from two LEO satellites such as Communication/Navigation Outage Forecast System (C/NOFS) and Gravity field and steady-state Ocean Circulation explorer (GOCE) and world geomagnetic field and solar terminator geomagnetic field line models. Figure 1 shows monthly and longitudinal variations of occurrence of ion density irregularity, vertical maximum drift velocity and zonal wind speed for the years 2011 (top panels) and 2012 (bottom panels). The first two columns, from the left, show the probability of occurrence of ion density perturbations for two threshold ion density perturbation values: $N>1\times10^{10}$ ions per m^3 and $N>2.5\times10^{10}$ ions per m^3, respectively. The monthly values of occurrence probability of ion density irregularities are computed by counting irregularities within 10^o longitude bins with respect to these threshold values whereas the drift velocity and zonal wind speed maps are obtained by averaging in these longitude bins (see 3^{rd} and 4^{th} columns of Figure 1). Interestingly, the monthly and longitudinal variations of zonal wind speed show similar patterns with maps of seasonal and longitudinal variations of drift velocity and occurrence of irregularity. The highest zonal wind speed is obtained in the same months and longitudes that the highest drift velocity and occurrence rates of irregularity.

To compare the effect of geomagnetic field strength, eastward zonal neutral wind

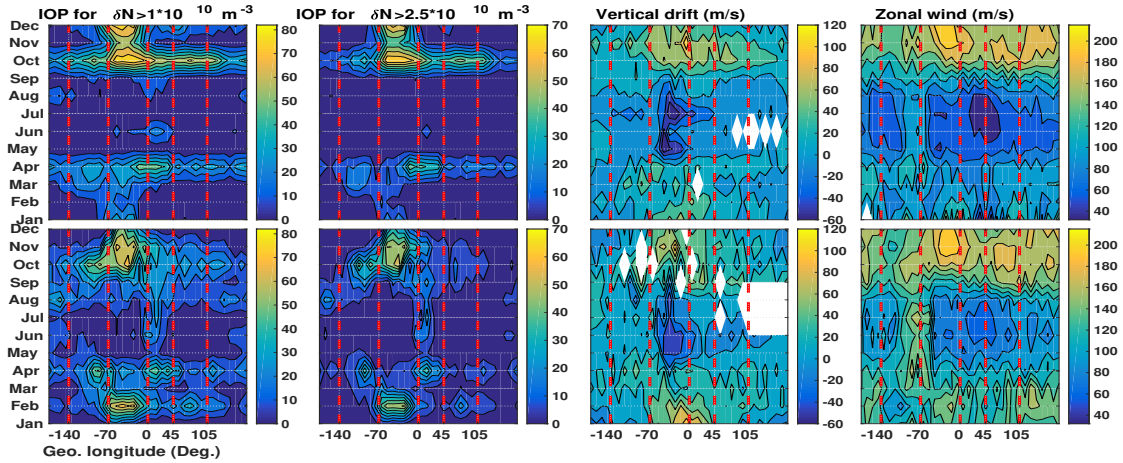

Figure 1: map of ion density perturbation occurrence (1st, 2nd columns for different ion density irregularity thresholds), maximum vertical drift velocity (3^{rd} column), and zonal wind speed (4^{th} panels) versus longitude and month for the years 2011 (top panels) and 2012 (bottom panels).

speed, and conductivity of the ionosphere on the longitudinal variations of vertical drift velocity, Figures 2 (for year 2011) is produced. The 1^{st}, 2^{nd}, 3^{rd}, and 4^{th} rows of Figure 2 show the longitudinal variations of vertical drift velocity, zonal neutral wind speed, geomagnetic field strength at the magnetic equator, and integrated Pederson conductivity, respectively.

In the left hand side panels of Figure 2, the longitudinal variations of the drift velocity (top panels) does not follow the longitudinal variations of zonal neutral wind speed (2^{nd} rows from the top) instead it follows the inverse of the geomagnetic field strength. This may be due to relatively high longitudinal variation of geomagnetic field strength compared to the zonal electric field that can be generated by zonal neutral wind speed (Eccles, et al., 2015) without much longitudinal variations. Conversely, as shown on the right-hand panels, the longitudinal variation of the drift velocity (top panels) does follow strongly the longitudinal variations of zonal neutral wind speed (2^{nd} rows from the top) instead of the geomagnetic field strengths. The zonal neutral wind speed in the right panels show clear difference with the one displayed in the left hand panels; the magnitude of zonal wind speeds shown in the right hand panels are stronger (U$>$ 150 m/s in most of the longitudes) and show larger longitudinal variations than the one in the left hand side panels (U$<$150 m/s and almost constant at all longitudes). This implies that strong eastward zonal neutral wind speed with considerable longitudinal variations may be the cause for strong electric field and vertical drift with similar longitudinal variations through ionosphere F-layer dynamo instead of the longitudinal variation of the geomagnetic field strength. A manuscript with these sample results are written and submitted for publication and now it is under review (M. Nigussie, M. B. Moldwin, S. Radicella, E. Yizengaw, S. Zou, B. Nava, *The effect of F-layer zonal neutral wind on the monthly and longitudinal variability of equatorial ionosphere irregularity and drift velocity.*

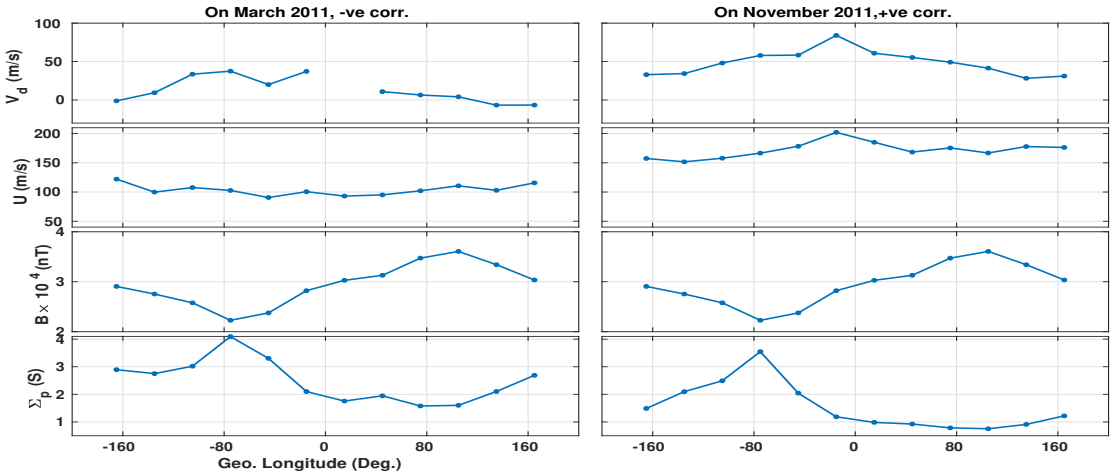

Figure 2: longitudinal variation of vertical drift velocity, zonal neutral wind, and geomagnetic field strength at magnetic equator, and height integrated Pederson conductivity (Σ_p), from top to bottom, for March (left) and November (right) 2011.

The other research objective is to investigate the role of atmospheric gravity waves in triggering the equatorial spread F. For this work, simultaneous atmospheric temperature perturbation profiles obtained from NASA's Thermosphere-Ionosphere-Mesosphere Energetic and Dynamics (TIMED) satellite and equatorial ion density and vertical plasma drift velocity observations with and without ESF activity obtained from C/NOFS satellite are used. The horizontal and vertical wavelengths of ionospheric oscillations and GWs are estimated applying wavelet analysis techniques. In addition, vertically propagating GWs that dissipate energy in the ionosphere-thermosphere system are investigated using spectral analysis technique. Sample results are shown in Figures 3 and 4. Figure 3 shows

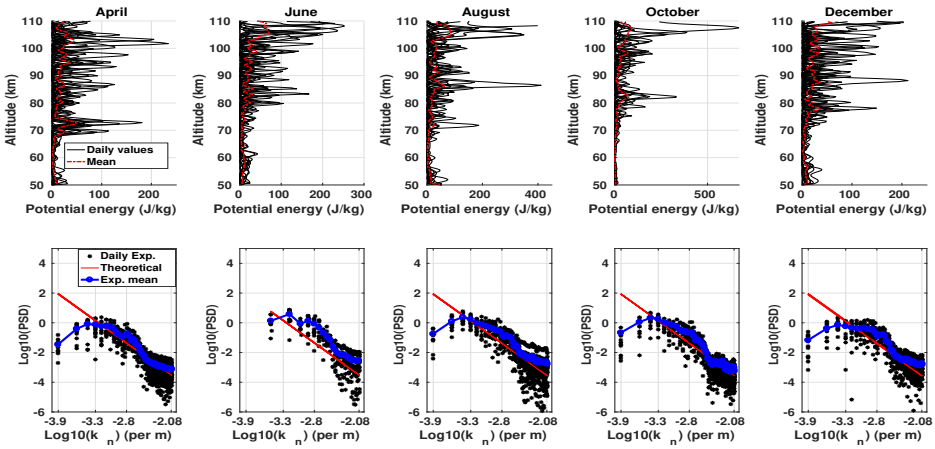

Figure 3: Gravity wave potential energy versus altitude (km) (top panels) and logarithm of theoretical and experimental PSD versus logarithm of vertical wave number (bottom panels) in the year 2013.

day-to-day activity of the gravity waves for 65 days in 2013. These days data have been obtained near to the magnetic equator at local times between 18 to 19 hours. The top panels show daily (black lines) and mean (red broken line) gravity wave potential energy versus altitude for each month. The day-to-day altitude variations of the potential energy show similar patterns within and across these months. As seen in the figure average potential energy for April, June, August, October, and December increase with altitude up to about 75, 80, 85, 80, and 80 km altitudes, respectively and then decreases (or not growing) with increasing altitude up to about 100 km. The logarithm of daily and mean experimental PSD of temperature fluctuations corresponding to the top panels of this figure and daily theoretical linear saturation of gravity waves PSD versus logarithm of vertical wave number are also shown in the bottom panels of the same figure. The PSD and vertical wave numbers are estimated corresponding to temperature fluctuations obtained above 90 km altitude. Very interestingly the experimental day-to-day values of the PSD within and among the months show similar patterns. The experimental mean PSD and the theoretical values show excellent agreement between -3.3 and -2.08 logarithm of vertical wave numbers that respectively correspond to 13 and 1 km vertical wavelength in all of the months. This indicates that gravity waves with vertical wavelengths between about 1 and 13 km are the one that dissipate energy at the heights above about 90 km in the ionosphere-atmosphere system. To compare the characterstics of atmopsheric gravity waves and oscillation of ion density, analysis has been done using data for the cases with and without ionospheic ion density irregularities. Figure 4 shows east-west oscillation characteristics of the ion density and atmospheric gravity waves both for the cases of irregular and non-irregular ionosphere. The first column in this figure show the ion den-

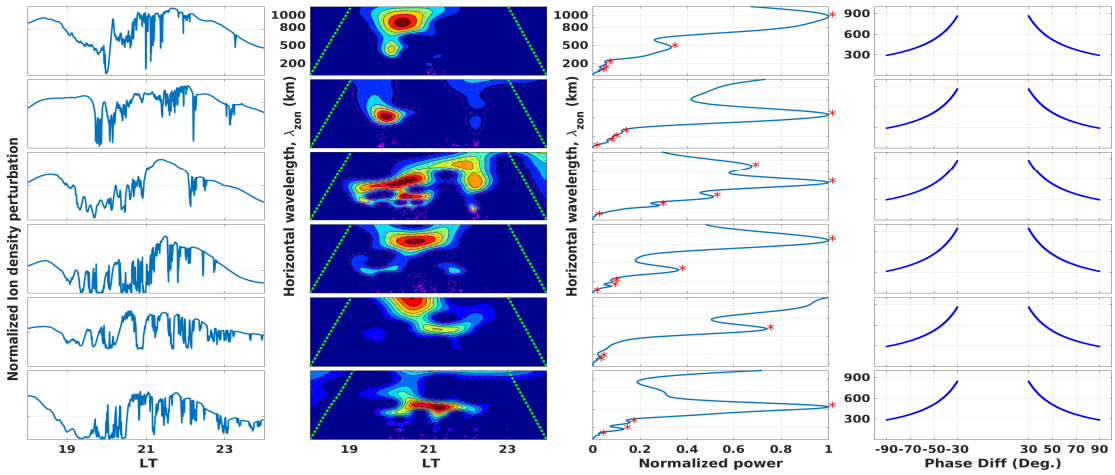

Figure 4: normalized ion density perturbation (left panels) versus LT, contour map of wavelet power of normalized ion density fluctuations versus zonal wave length and LT (2nd column from the left) and time integrated normalized wavelet power of normalized ion density fluctuations versus zonal wavelength (3rd column from the left), gravity wave zonal wavelength versus phase shift (4th column from the left) on 15 October 2011.

sity perturbation versus local time, the panels in second and the third columns, from the left, show the wavelet transform power of the ion density perturbations versus zonal

wavelength and local time and normalized global wavelet power spectrum (GWPS) as a function of the zonal wavelength, respectively. The fourth column, from the left, shows the east-west component of the horizontal wavelength of atmospheric gravity waves estimated from pair of temperature profiles versus phase shift angle. The characterstics of atmospheric gravity waves for the cases of with and without ionospheric irregularity are similar. In summary, we find that vertical wavelength of GW, corresponding to dominant wavelet power, ranges from 12 to 31 km regardless of the conditions of the ionosphere; however, GWs with vertical wavelengths between about 1 to 13 km are found every day saturated between 90 and 110 km at different longitudinal sectors. Filtering out vertical wavelengths above 13 km from temperature perturbations, ranges of zonal wavelengths of GW (i.e. from about 290 to 950 km) are found corresponding to irregular and non-irregular ionosphere. Similarly, corresponding to dominant oscillations, zonal wavelength of ion density perturbations is found within 16 to 1520 km. Moreover, we find an excellent agreement among the median zonal wavelengths of GW for the cases of irregular and non-irregular ionosphere and ion density perturbations that are 518, 495, and 491 km, respectively. The results imply that seed perturbations due to GW with vertical wavelength from about 1 to 13 km evolve to ion density irregularity and may be amplified due to post-sunset vertical upward drift velocity. A manuscript with these sample results are written and submitted for publication and now it is under review (M. Nigussie, M. B. Moldwin, E. Yizengaw, K. Groves, *Investigating the role of gravity waves on equatorial ionospheric irregularities using TIMED/SABER and C/NOFS satellite observations.*

Figure 5 shows preliminary result on the correlation between occurence of ionopsheric irregularity (left), vertical drift velocity (middle), and minimum values of potential energy of gravity waves within altitudes from 80 to 100 km (right). As seen in the months and longitudes with relatively high minimum potential energy of GW, the occurence proability and vertical drift velocity are low. This result will be refined further and it will be considered as continuation study.

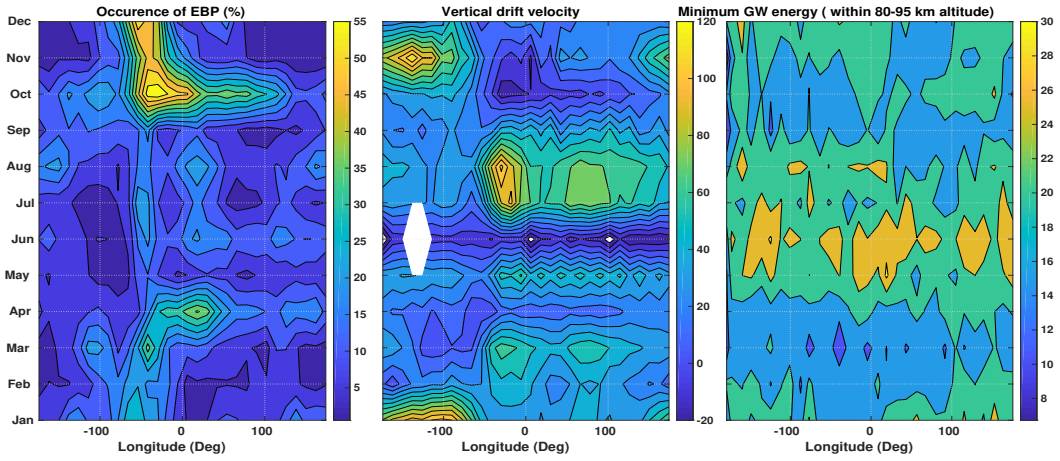

Figure 5: map of ion density perturbation occurrence (left), vertical drift velocity (middle), and minimum potential energy within altitudes from 80 to 100km (right) versus longitude and month for the years 2011.

The daytime and nighttime equatorial electrodynamics have distinct behavior. The well known daytime phenomena are equatorial ionization anomaly (EIA) and equatorial electrojet (EEJ). Some authors have tried to associate these phenomena to the generation or suppression of equatorial post-sunset ionospheric irregularities; however, for East African region this kind of study has not been done due to lack of ground based instruments in the region. In this project, as we have magnetometers and ionospheric monitoring systems such as GPS receivers recently in the region, the effect of EIA and EEJ during quiet and distributed time has been investigated. Seba and Nigussie (2016) have investigated the triggering and inhibition mechanism of equatorial ionospheric irregularity using scintillation index (S4), EEJ, interplanetary electric field (IEFy), symH index, AE index, and Bz on five selected storm and two not-storm days. As sample Figure 6 shows quiet time variation of TEC and parameters mentioned above on the days of 16-18 March 2011. From the analysis in this study it is found that when the east-ward

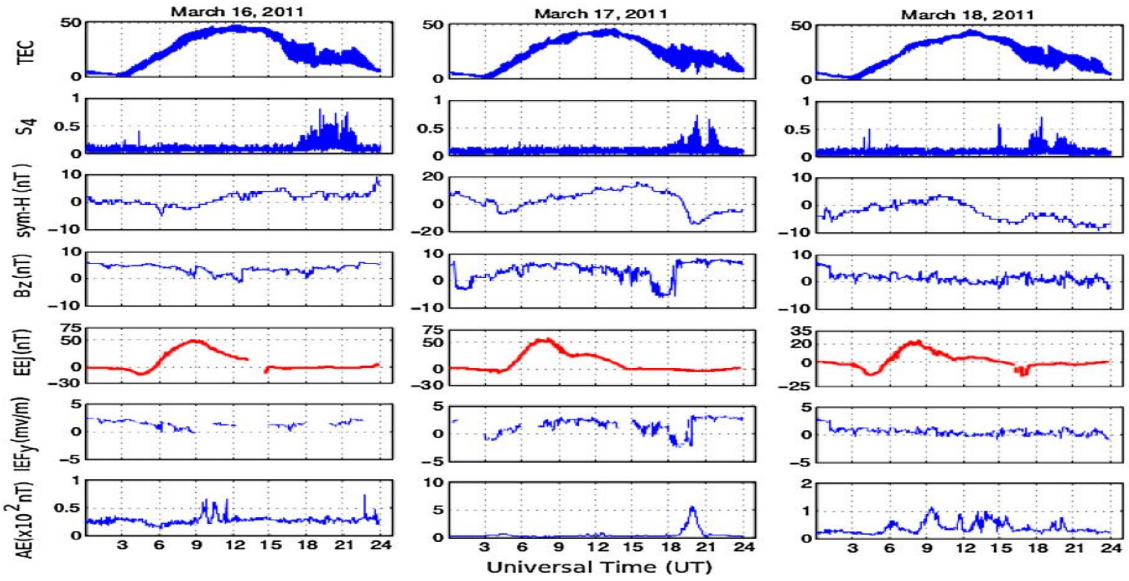

Figure 6: geomagneticaaly quiet day pattern of TEC and S4 and their association to symmH, Bz, EEJ, IEFy and AE on March 16-18, 2011.

EEJ fluctuates in magnitude due to storm time induced electric fields at around noontime, the post-sunset scintillation is inhibited. All observed post-sunset scintillation in equinox season are resulted when the daytime EEJ is non fluctuating. Detail analysis and results are found in Seba and Nigussie (2016).

The relationship between EIA and equatorial post sunset ionopsheric irregularity in East African region has been also investigated. This investigation has been done using ground based chain of GPS receivers and neutral wind model data. From these data different parameters such as anomaly strength, symmetry of anomaly crests, wind speed magnitude and direction, and magnitude of rate of TEC index (ROTI) have been computed and analysed, for example, sample results are shown in Figure 7. From analysis done for this study it is found that mean crest to trough ratio (CTR) greater than or equal to 1.4 and mean north crest to south crest ratio (CCR) within 0.9 and 1.1 in the time

between 19 LT and 21LT are taken as good conditions for the occurnce of irregularity. Detail analysis and results are found in Seba et al. (2018).

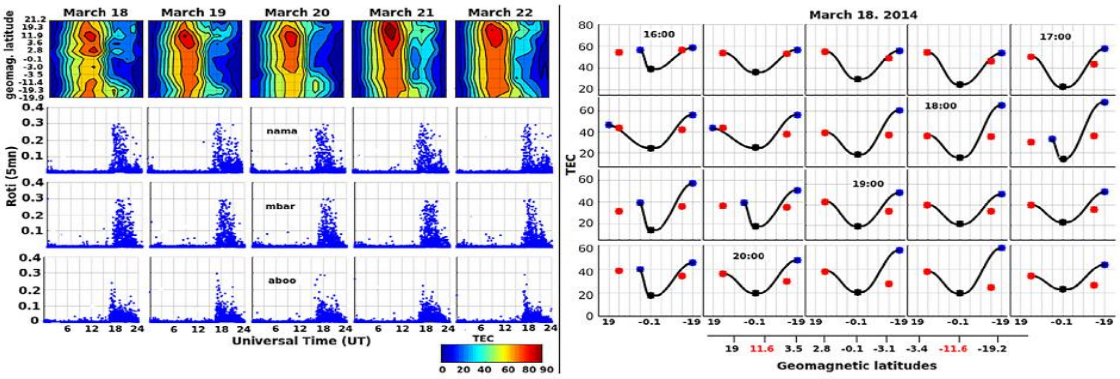

Figure 7: The left side upper five panels over ROTI plots are one hour averagred TEC plots from 11 GPS stations on 18-22 March and the right plots are 15-min averaged TEC from 16:00 UT to 20:45 UT on 18 March 2014.

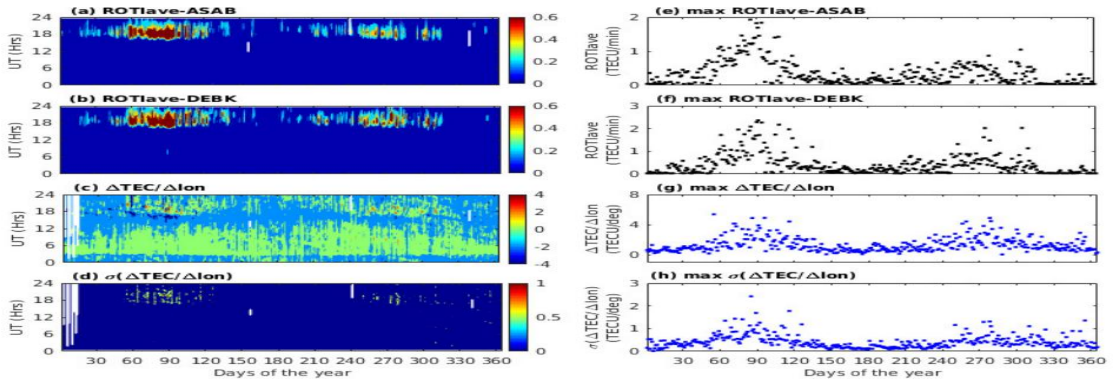

Figure 8: Annual and daily maximum value variation of (a,b) ROTI_{ave} over Asab (ASAB), (c,d) ROTI_{ave} over Debark (DEBK), (e,f) spatial gradient of TEC ($\frac{\Delta TEC}{\Delta lon}$), (g, h) standard deviation of $\frac{\Delta TEC}{\Delta lon}$ in the year 2014, LT=UT+3 hrs.

It is well known that the post-sunset equatorial ionospheric irregularity is mainly controlled by plasma vertical drift velocity that directly depends on the PRE electric field. The enhancement of east-ward electric field (PRE) is believed to be due to sharp zonal gradient of electron density around the solar terminator at the bottom-side of the F-layer of the ionosphere. Knowing the magnitude of PRE that can trigger irregularity is very important for understanding the dynamics of the post-sunset ionosphere; however, as its magnitude is very small noise can mask it and hence we may not get proper measurement of PRE electric field. This implies that we need to have an alternative indicator of the PRE. As TEC is the integral of electron density between the positions of GPS satellite and receiver on the ground, taking the gradient of TEC collected by GPS receivers installed almost in the same latitude but at different longitude around solar terminator could provide good indicator of the PRE. This idea, supported by EOARD,

has been demonstrated and sample results are shown in Figure 8. As seen in this figure, the diurnal pattern of ionospheric irregularity (ROTI values) and spatial gradient of TEC have shown similar pattern. This work has been written in manuscript form and submitted for publication, now it is under review (title of manuscript: Spatial gradient of total electron contnent (TEC) between two nearby stations as indicator of occurrence of ionopsheric irregularity: T. Dugassa, J. B. Habarulema, M. Nigussie).

As the neutral wind and ionospheric dynamics are linked with each other, one of PhD students has done characterization of the thermospheric neutral wind parameters using data from FPI installed at Bahir Dar. Sample results on local time variation of zonal and meridional neutral wind speeds are shown in Figure 9. The first results of FPI-measured monthly-averaged equatorial vector winds and temperature obtained over a period of 6 months in the African longitudinal sector shows several differences relative to similar results obtained in other longitude sectors. Detail about the results of this study is found in Tesema et al. (2017).

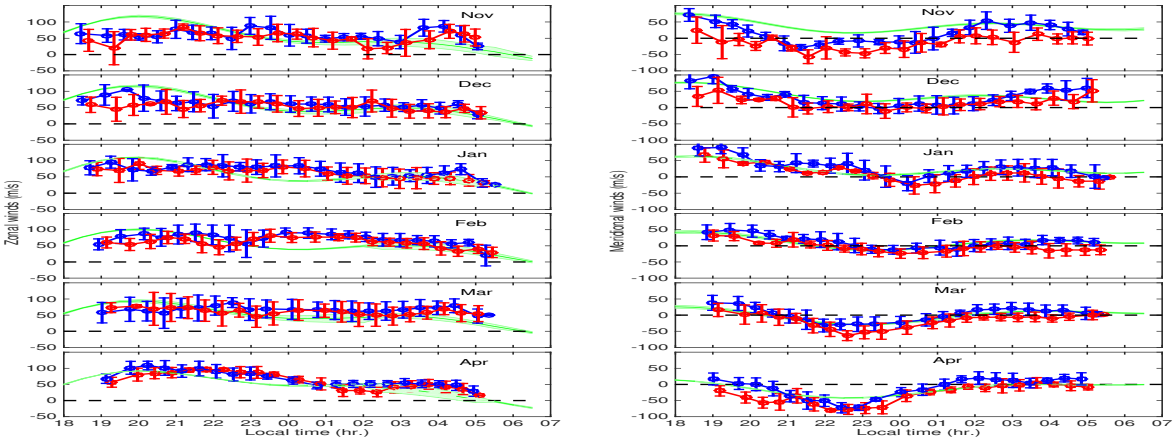

Figure 9: Monthly-averaged winds between November 2015 and April 2016 for a time bin of 30 min. The left panel shows the zonal wind data for east (blue) and west (red) directions. The right panel shows the meridional wind data for north (blue) and south (red) directions. Also shown are the HWM14 model results (green) for the zonal and meridional speed variations averaged for the nights included in each month. The thickness for each model curve indicates the range of variability. The vertical bar shows the overall range of variation within each averaging bin.

2.2 Modeling of the equatorial ionospheric and solar parameters

The variability of the ionosphere is described by the variability of its parameters such as TEC, electron density, plasma drift velocity, and so on. This implies that modeling ionospheric parameters is very useful to mitigate the effect of the ionosphere on propagating trans-ionospheric radio waves and also get better understanding of the dynamics of the ionosphere. For these purposes ionospheric empirical models have been developed by the other authors using data mainly from the mid-latitude of the northern hemisphere. NeQuick 2 and International Reference Ionosphere (IRI) are examples of climatological

electron density and TEC models. As these are global models their performances need to be assessed using whenever new ionospheric observations are available, especially for the low and high latitude regions. This kind of works are among the objectives that have been designed in this project. A technique to estimate near-real-time electron density has been developed. This has been done by assisting the NeQuick 2 model using ground-based TEC at low and high latitude regions. Sample results are shown in Figures 10 and 11. Figure 10 shows the electron density profiles that are computed before (green dotted curves) and after (blue solid curves) model adaptation corresponding to C/NOFS observations (pink dots) obtained when the satellite was below 420 km altitude. This has been done to get general understanding about the accuracy of the model in reproducing the electron density near the F2 peak. Figure 11 has shown electron density profiles

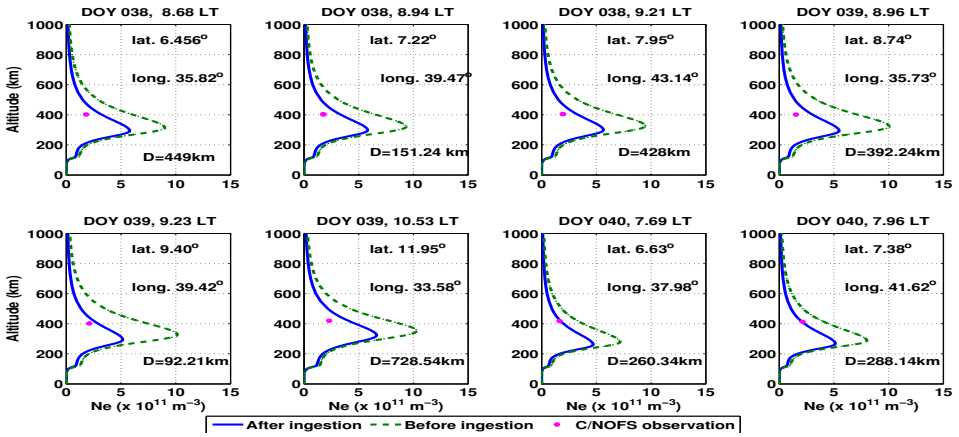

Figure 10: Altitude profile of the modeled electron density before and after adaptation and point value of C/NOFS observation.

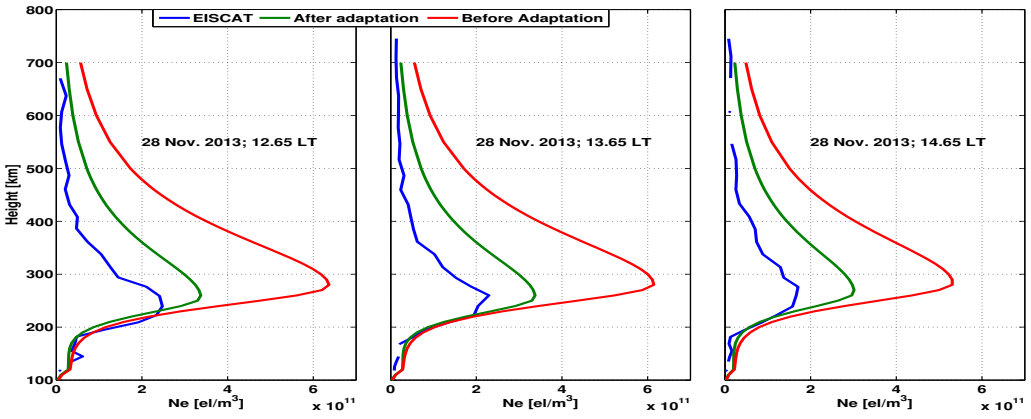

Figure 11: EISCAT VHF radar measured and NeQuick 2 modeled (before and after adaptation) electron density profile on 28 November 2013.

estimated on 28 November 2013 before and after model adaptation to GPS receiver installed at Tromsø and from EISCAT VHF radar. The radar measurements shown in this

figure has been obtained at 1 min integration. As it is depicted in Figures 10 and 11 considerable improvement in the model performance has been obtained in reproducing the topside profile and F2 peak electron density and height when the model is adapted to GPS sTEC. These and similar results are published and found in Nigussie et al. (2016). Similarly, Neural network (NN) technique has been applied to model and forecast iono-

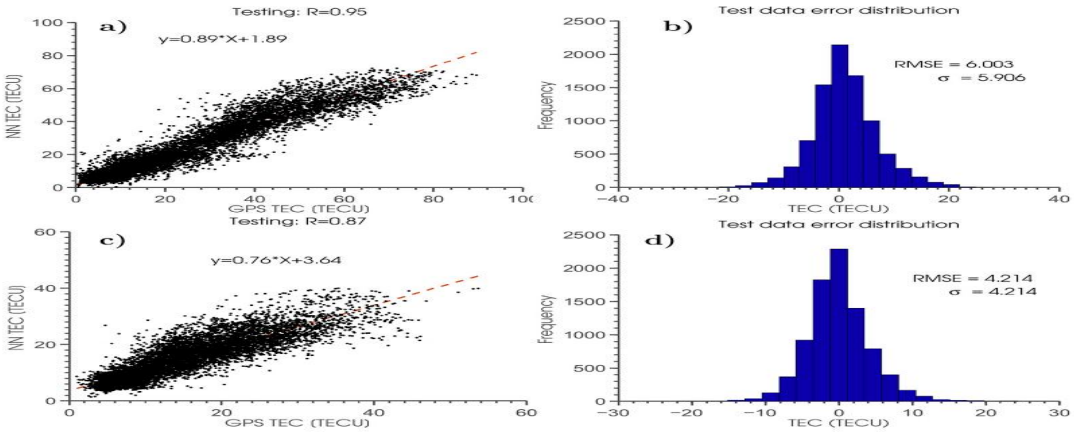

Figure 12: scatter plots NN modeled versus observed TEC for Armi (a) and Ebre (c) stations and the correspondisng distribution of mis-modeling.

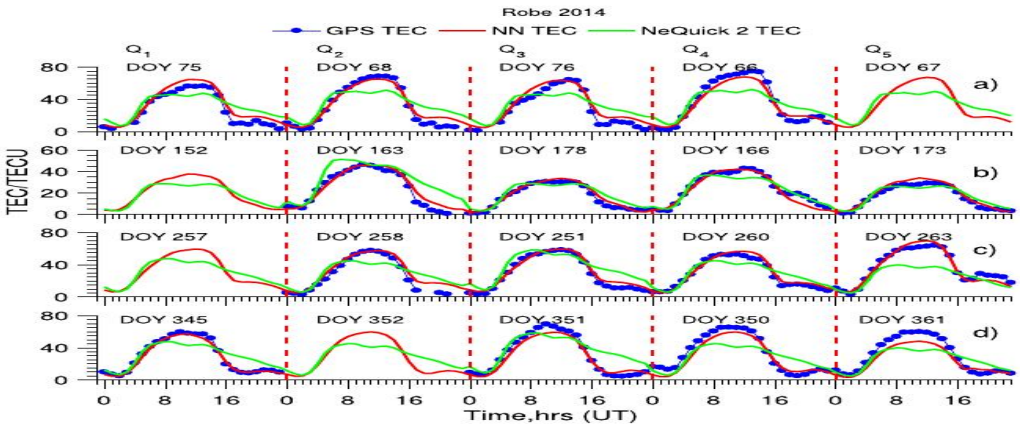

Figure 13: Diurnal variation of NN and NeQuick modeled and GPS observed TEC in the year 2014.

spheric TEC (Tebabal et al., 2019 and 2018). Sample results are shown in Figures 12 and 13. Left panels of Figure 12 show the scatter plots of NN modeled TEC versus the GPS-TEC observation for the year 2015. The right panels also show distribution of the mis-modeling between NN modeled and GPS observed TEC. As seen in these panels the RMSE is found below about 6 TECu. Figure 13 shows diurnal NN and NeQuick 2 modeled and GPS observed TEC for the station Robe. As seen NN modeled TEC best follow the trend of observed TEC. These and similar results are published and found in Tebabal et al. (2018) and (2019).

In a separate work, the performance of empirical model of vertical drift velocity have been assessed against C/NOFS observation and also proposed a simplified vertical drift velocity model based on basic physics laws such as Ampere's and Ohm's laws. The existing empirical and new models performance have been evaluated with respect to C/NOFS observations. Sample results are shown in Figure 14. As seen in the right panels of this figure, the new model (denoted by PVD) performs better than the other two empirical models. This and similar results are written in manuscript form and submitted for publication and now it is accepted with minor revision (it is entitiled: A method of estimating equatorial plasma vertical drift velocity and its evaluation using C/NOFS observations: H. Marew, M. Nigussie, D. Hui, B. Damtie).

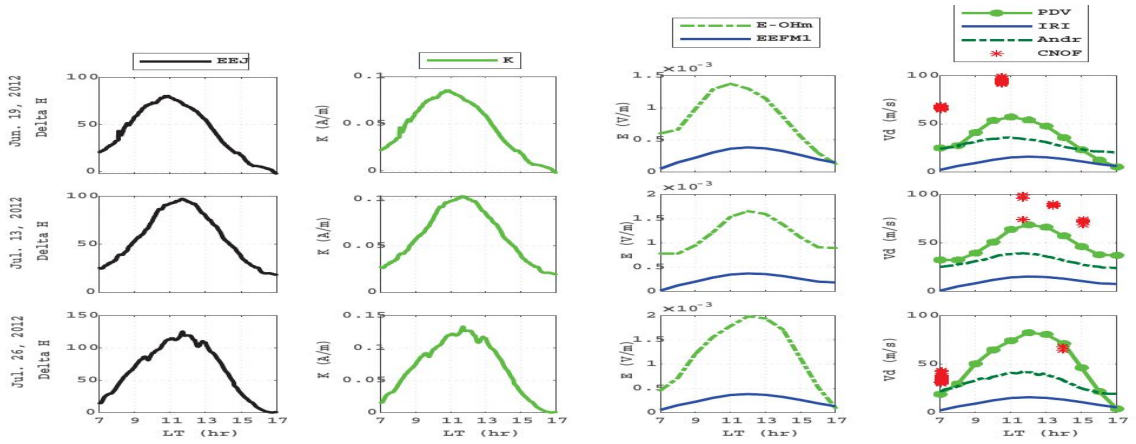

Figure 14: Daytime EEJ, estimated sheet current density, E-field ad vertical ion drift velocity over Jicamarca Radio Observatory, Peru on 19 June13 and 26 2012.

The remaining works supported by this grant are listed below together with the once mentioned above.

2.3 List of publications obtained supported by this grant

1. **Melessew Nigussie**, Mark B. Moldwin, Sandro Radicella, Endawoke Yizengaw, Shasha Zou, Bruno Nava, The effect of F-layer zonal neutral wind on the monthly and longitudinal variability of equatorial 2 ionosphere irregularity and drift velocity, **u**nder review

2. **Melessew Nigussie**, Mark B. Moldwin, Endawoke Yizengaw, Keith Groves, Investigating the role of gravity waves on equatorial ionospheric irregularities using TIMED/SABER and C/NOFS satellite observations, **under review**.

3. **Melessew Nigussie**, Investigation of the Characteristics of wavelike oscillations of post-sunset Equatorial Ionospheric Irregularity by Decomposing Fluctuating TEC, **it is being modified**.

4. **H. Marew**, **Melessew Nigussie**, D. Hui, **B. Damtie**, A new method of estimating equatorial plasma vertical drift velocity and its evaluation using C/NOFS

observations, **accepted with minor revision**

5. T. Dugassa, J. B. Habarulema, **M. Nigussie**,spatial gradient of total electron content (TEC) between two nearby stations as indicator of occurance of ionospheric irregularity, **under review**.

6. **A. Tebabal**, S. M. Radicella, **B. Damtie**, Y. Migoya-Orue, **M. Nigussie**, B. Nava (2019), Feed forward neural network based ionopsheric model for the East Africa, Journal of atmospheric and solar terresterial physics, 191, 105052.

7. **A. Tebabal**., S. M. Radicella, **M. Nigussie**, **B. Damtie** (2018), Local TEC modeling and forecasting using neural networks, Journal of atmospheric and solar terresterial physics, 172, 143-151.

8. Mengistu, E., **B. Damtie**, M. B. Moldwin, **M. Nigussie** (2018), Comparison of GPS-TEC measurements with NeQuick2 and IRI model predictions in the low latitude East African region during varying solar activity period (1998 and 2008-2015) Advances in Space Research DOI: 10.1016/j.asr.2018.01.009

9. Seba E. B., **M. Nigussie**, Mark M. Moldwin (2018), The relationship between equatorial ionization anomaly and nightime equatorial spread F in east Africa, Advances in Space Research, https://doi.org/10.1016/j.asr.2018.06.029.

10. Seid, A. M., Kendeya, T. B., L., Roininen, **M. Nigussie** (2018) Hierarchical Bayesian modeling of ionospheric TEC disturbances as non-stationary processes, Advances in Space Research, DOI:10.1016/j.asr.2017.12.009

11. **Tesema F.**, R. Mesquita, J. Meriwether, **B. Damtie**, **M. Nigussie**, J. Makela, D. Fisher, B. Harding, E. Yizengaw, S. Sanders (2017), New results on equatorial thermospheric winds and temperatures from Ethiopia, Africa, Annalus Geophysicae., 35, 333-344.

12. **Kassa T.**, **B. Damtie** (2017), Ionospheric irregularity over Bahir Dar Ethiopia during selected geomagnetic storms, advances in space research, http://dx. doi.org/10.1016/j.asr.2017.03.036

13. **Kassa T.**, S. Tilahun **B. Damtie**, (2017) Solar activity indices as a proxy for the variations of ionospheric Total electron contnent (TEC) over Bahir Dar, Ethiopia during the year 2010-2014, advances in space research, http://dx. doi.org/10.1016/j.asr.2017.06.024

14. **Tebabal, A.**, **B. Damtie**, **M. Nigussie**, E. Yizengaw, (2017) Temporal variations of solar irradiance since 1947, Solar Physics, 292: 112. https://doi.org/10.1007/s11207-017-1128-x

15. **Nigussie, M.**, S. Radicella, **B. Damtie**, E. Yizengaw, B. Nava, L. Roininen (2016), Validation of NeQuick TEC data ingestion technique against C/NOFS and EISCAT electron density measurements, Radio Science, 51, 7, 905–917 DOI: 10.1002/2015RS005930

16. Beshire, E., **M. Nigussie** (2016), Investigating the effect of geomagnetic storm and equatorial electrojet on equatorial ionospheric irregularity over East African sector, Advances in Space Research, http://dx.doi.org/10.1016/j.asr.2016.06.037

3 Other activities done supported by grant FA9550-16-1-0070

3.1 Conference participation

Supported by this grant students and researchers have particpated in differnt conferences such as AGU 2017 and 2018 fall meeting (see for example left photo in Figure 15). The PI of this project has won AGU 2017 Africa Award for Research Excellence in Space Science (right photo in Figure 15). This grant was contributed a lot for the selection of the PI for this award.

Figure 15: sample photo at AGU fall meeting (left) and photo during AGU 2017 Africa Award for Research Excellence in space science (right).

3.2 PhD student training

The other indirect aim of the project was to train PhD students in space physics at Bahir Dar university. Supported by this grant Dr Ambelu Tebabal has defended successfully his PHD thesis in Februry 2018 at Bahir Dar University, Ethiopia (see Figure 16).

Figure 16: Dr Ambelu during thesis defence (left) and audience and his opponents (right).

4 References

- M. Nigussie, Mark B. Moldwin, Sandro Radicella, Endawoke Yizengaw, Shasha Zou, Bruno Nava, The effect of F-layer zonal neutral wind on the monthly and longitudinal variability of equatorial 2 ionosphere irregularity and drift velocity, **under review manuscript**

- M. Nigussie, Mark B. Moldwin, Endawoke Yizengaw, Keith Groves, Investigating the role of gravity waves on equatorial ionospheric irregularities using TIMED/SABER and C/NOFS satellite observations, **under review manuscript**.

- H. Marew, M. Nigussie, D. Hui, B. Damtie, A new method of estimating equatorial plasma vertical drift velocity and its evaluation using C/NOFS observations, **accepted with minor revision.**

- T. Dugassa, J. B. Habarulema, M. Nigussie,spatial gradient of total electron content (TEC) between two nearby stations as indicator of occurance of ionospheric irregularity, **under review manuscript**.

- A. Tebabal, S. M. Radicella, B. Damtie, Y. Migoya-Orue, M. Nigussie, B. Nava, (2019) Feed forward neural network based ionopsheric model for the East Africa, Journal of atmospheric and solar terresterial physics, 191, 105052.

- A. Tebabal., S. M. Radicella, M. Nigussie, B. Damtie, (2018), Regional TEC modeling and forecasting using neural networks, Journal of atmospheric and solar terresterial physics, 172, 143-151.

- Seba E. B., M. Nigussie, Mark M. Moldwin, (2018), The relationship between equatorial ionization anomaly and nightime equatorial spread F in east Africa, Advances in Space Research, https://doi.org/10.1016/j.asr.2018.06.029.

- Tesema F., R. Mesquita, J. Meriwether, B. Damtie, M. Nigussie, J. Makela, D. Fisher, B. Harding, E. Yizengaw, S. Sanders, (2017) New results on equatorial thermospheric winds and temperatures from Ethiopia, Africa, Ann. Geophy., 35, 333-344.

- Nigussie, M., S. Radicella, B. Damtie, E. Yizengaw, B. Nava, L. Roininen, (2016), Validation of NeQuick TEC data ingestion technique against C/NOFS and EISCAT electron density measurements, Radio Sci., 51, 7, 905–917 DOI: 10.1002/2015RS005930

- Beshire, E., M. Nigussie, (2016), Investigating the effect of geomagnetic storm and equatorial electrojet on equatorial ionospheric irregularity over East African sector, Adv. Space Res. (2016), http://dx.doi.org/10.1016/j.asr.2016.06.037

- Eccles, J. V., J. P. St. Maurice, R. W. Shunk, (2015), Mechanism underlying the prereversal enhancement of the vertical plasma drift in the low latitude ionosphere, Journal o Geophysical Research, 120, 4950-4970, doi:10.1002/2014JA020664.

- Hei, M. A., R. A. Heelis, J. P. McClure (2005), Seasonal and longitudinal variation of large-scale topside equatorial plasma depletions, J. Geophys. Res. 110, A12315, doi:10.1029/2005JA011153.

- Huang, C.-S., and M. R. Hairston (2015), The postsunset vertical plasma drift and its effects on the generation of equatorial plasma bubbles observed by the C/NOFS satellite, J. Geophys. Res. Space Physics, 120, 2263–2275, doi:10.1002/2014JA020735.

- Rishbeth, H. (1971), The F-layer dynamo, Planet. Space Sci., 19, 263–267, doi:10.1016/0032 0633(71)90205-4.

- Tsunoda, R. T. (2010), On seeding equatorial spread F during solstices, Geophys. Res. Lett., 37, L05102, doi:10.1029/2010GL042576.

- Tsunoda, R. T. (1985), Control of the seasonal and longitudinal occurrence of equatorial scintillation by the longitudinal gradient of in integrated E region conductivity, J. Geophys. Res., 90, 447-456.

- Su, S.-Y., C. K. Chao, and C. H. Liu (2006), On monthly/seasonal/longitudinal variations of equatorial irregularity occurrences and their relationship with the post-sunset vertical drift velocities, J. Geophys. Res., 113, A05307, doi:10.1029/2007JA012809

- Kelley, M. C., M. F. Larsen, C. LaHoz, J. P. McClure, (1981), Gravity wave initiation of equatorial spread F: A case study, J. Geophys. Res. 109, 86, 90987-9100.

- Sultan P. J., (1996) Linear theory and modeling of the Rayleigh-Taylor instability leading to the occurrence of equatorial spread F, J. Geophys. Res., 101, A12, 875-891.

- Mendillo, M., J. Baumoardner, X. PI, P. J. Sultan, R. Tsunoda (1992) Onset Conditions for Equatorial Spread F, J. Geophys. Res., 97, A9, 865-876.